

# The influence of geometry and topology of quantum graphs on their nonlinear-optical properties

Rick Lytel, Shores Shafei, Julian H. Smith and Mark G. Kuzyk

*Department of Physics and Astronomy, Washington State University, Pullman, Washington 99164-2814\**

(Dated: July 27, 2012)

We analyze the nonlinear optics of quasi one-dimensional quantum graphs and manipulate their topology and geometry to generate for the first time nonlinearities in a simple system approaching the fundamental limits. Changes in geometry result in smooth variations of the nonlinearities. Topological changes between geometrically-similar systems cause profound changes in the nonlinear susceptibilities that include a discontinuity due to abrupt changes in the boundary conditions. This work may inform the design of new molecules or nano-scale structures for nonlinear optics.

PACS numbers: 42.65.An, 78.67.Lt

## I. INTRODUCTION

A quantum graph is a network of edges and vertices upon which particle motion is described by a Hamiltonian with a complete set of eigenstates, an energy spectrum, and flux-conserving boundary conditions [1]. An electron on the graph is assumed to be tightly bound in the transverse direction, yielding a quasi one-dimensional dynamical system. When coupled to optical fields, this system is a model of nonlinear optical molecular structures exhibiting rich topological and geometrical properties.

Quantum graphs with bare and dressed edges have been solved using periodic orbit theory and extensively studied for their statistical properties and energy spectra [1–7]. This letter is the first to apply quantum graph models to nonlinear optics by calculating the hyperpolarizabilities (first and second) using explicit expressions for the eigenstates and energy spectra. We employ bare graphs which use free-particle states  $A_{ij} \sin(ks_{ij} + \phi_{ij})$  for each edge connecting vertex pairs  $i, j$ , flux conservation at each degree  $> 1$  vertex, and Dirichlet boundary conditions at terminal vertices.

In order to compare the hyperpolarizabilities of quantum graphs of differing size, we normalize each to the fundamental limit [8] to yield the intrinsic first ( $\beta$ ) and second ( $\gamma$ ) hyperpolarizability. Unless otherwise stated, all values presented here are intrinsic. Secondly, we define the molecular  $x$ -axis along the direction such that  $\beta_{xxx}$  is maximum. It is typical for  $\beta_{xxx}$  and  $\gamma_{xxx}$  to be largest along different axes, so the coordinate system for describing each may be and usually is different. The coordinate axis will be specified only when needed.  $\beta_{xxx}$  ( $\gamma_{xxx}$ ) should be understood as the largest  $x$ -diagonal tensor component of the intrinsic first (second) hyperpolarizability.

The calculation of the first and second hyperpolarizability requires a sum over states of products of the dipole matrix elements of the graph, divided by energy denom-

inators [9]. We use a quasi-one dimensional model where the electron is tightly confined to move along the edges by a transverse well of infinite height and zero width. As shown in [10], the residual effects of the vanishing transverse dimension are present in the Thomas-Reich-Kuhn (TKR) sum rules but drop out of the hyperpolarizabilities. We verified the correctness of our solutions by calculating both longitudinal and transverse contributions to the sum rules, as well as by showing how they contribute to the dipole-free sum-over-states formalism [11], so transverse contributions could be omitted from the calculation of the hyperpolarizability tensors.

The first hyperpolarizability  $\beta_{ijk}$  is a fully-symmetric, third rank tensor for planar graphs far from resonance, with four nonzero components and an invariant norm  $|\beta|$ . The second hyperpolarizability is likewise fully-symmetric in this limit and has five nonzero components and an invariant norm  $|\gamma|$ . The norms are given by

$$|\beta| = \sqrt{\beta_{xxx}^2 + 3\beta_{xxy}^2 + 3\beta_{xyy}^2 + \beta_{yyy}^2} \quad (1)$$

$$|\gamma| = \sqrt{\gamma_{xxxx}^2 + 4\gamma_{xxxy}^2 + 6\gamma_{xxyy}^2 + 4\gamma_{xyyy}^2 + \gamma_{yyyy}^2}.$$

and contain all of the nonlinear optical physics of the model. Each tensor component in Eq. (1) may be calculated using a sum-over-states expression once the dipole moment matrix has been determined.[9, 12]

The computation of the contributions to the dipole moment matrix over the edges of the graph is straightforward and when summed results in a set of matrix elements for the entire graph, from which hyperpolarizabilities may be calculated with the usual sum-over-states expansions,[9, 12] normalized by their maximum intrinsic values [10]. For the position of the charge in the wire,  $x$ , we find that

$$x_{nm} = \sum_i \cos \theta_i K_{nm}^i, \quad (2)$$

where  $i$  is summed over all edges of the graph, and  $\theta_i$  is the angle between the segment  $i$  and the external  $x$ -axis. A similar expression holds for  $y_{nm}$  with  $\cos \theta_i \rightarrow \sin \theta_i$ . The factor  $K_{nm}^i$  is an integral on edge  $i$  of the product of the  $\psi_n^*$  and  $\psi_m$  energy eigenfunctions on the edge times

\* email: kuz@wsu.edu

the longitudinal coordinate on the edge, with each  $K_{nm}^i$  depending solely on the lengths and eigenfunctions on the edges. The number of eigenfunctions, their degeneracies (if any), and the energy spectra are fixed by the boundary conditions imposed by the topology of the graph. The angular factors in Eq. (2) describe the geometry of the graph and are identical for graphs with identical geometries but different topologies, such as a closed-loop triangle graph and a triangle graph with identical shape but one open vertex.

By analyzing classes of graphs with similar geometry but different topology, and vice-versa, we can extract both the topological and geometrical effects on the non-linear optics of the graph. For example, the diagonal component of the first hyperpolarizability tensor will always take the form

$$\beta_{xxx} = \sum_{i,j,k} (\cos \theta_i \cos \theta_j \cos \theta_k) \times A_{ijk},$$

$$A_{ijk} = \sum_{n,m} \frac{K_{0n}^i \bar{K}_{nm}^j K_{m0}^k}{E_n E_m}. \quad (3)$$














Equation (3) expresses the influence of the angular factors describing the geometry of the graph on each segment's contribution to the underlying quantum mechanics of the full graph as embodied in the edge factors  $K_{nm}^i$ . It is thus reasonable to speak of the cosine factors as the geometric specifiers. Since the topology of the graph determines the boundary conditions on the eigenstates, topological effects originate solely in  $A_{ijk}$ .

$A_{ijk}$  has three indices that couple the angular factors in ways that are determined by the topology of the graph, not its geometry. This means that the differences between a closed loop triangle and one with an open vertex arises from the quantum states, i.e., the topology of the graph. Along the edges of the graph, the electron knows nothing about angles; it only knows about the value of its wavefunction on any particular edge.

Table I displays the four sets of graphs studied. The first set are bent wires with different geometries but linear topology. The second set are the topologically-equivalent closed-loop graphs – again with different geometries. Below the double line, the next set are graphs with the same triangle geometry but which differ in topology. The final set are 3-prong irregular (i.e. irrational length ratios) star graphs, which are geometrically equivalent, but topologically distinct.

We generated tens of thousands of random configurations of each type of graph, and calculated the hyperpolarizability tensors for every sample. The simplest graph in the first topologically equivalent set is the line segment shown in the first row of Table I, and is characterized by vanishing  $\beta_{xxx}$  by virtue of its centrosymmetry, and by  $\gamma_{xxx} = -0.126$ . A bent wire, as shown in the second row of Table I, is topologically equivalent to the line but of different geometry (i.e. shape). Figure 1 shows the calculated hyperpolarizability for a bent wire that is formed by connecting the points (0,0), (x,y) and (1,0).

TABLE I. Effects of geometry and topology in simple graphs.

Graph	Geometry	Topology	$ \beta_{xxx} $	$\gamma_{xxx}$
	Line	Line	0.000	-0.126
	Bent Wire	Line	0.172	-0.126 to 0.007
	Triangle	Loop	0.049	-0.138 to 0
	Simple Quadrangle	Loop	0.056	-0.138 to 0
	All Quadrangles	Loop	0.072	-0.138 to 0
	All Quintangles	Loop	0.072	-0.138 to 0
	Triangle	Loop	0.049	-0.138 to 0
	Triangle	Line	0.133	-0.064 to 0.006
	Triangle	Line	0.172	-0.086 to 0.007
	Triangle	Line	0	-0.114 to 0
	3-star	3-Fork	0.55	-0.137 to 0.30
	3-star	Line	0.172	-0.126 to 0.007
	3-star	Line	0	-0.126 to 0

The largest hyperpolarizability is given by  $|\beta| = 0.172$  for a wire with  $(x, y) = (1.85, 0)$ . Similarly, the second hyperpolarizability varies from -0.126 to +0.007. This shows how the hyperpolarizability smoothly varies from zero for the straight wire and peaks for a bent wire that turns back on itself. For the case of  $\gamma_{xxx}$ , the best shape is given by an acute angle with vertex (0, 0) and endpoints (1, -1) and (1.8, 0). Despite their simplicity, bent wires have an intrinsic first hyperpolarizability that is about 17% of the fundamental limit. In contrast, most of the best molecules fall a factor of 30 short of the limit.[13]

Adding a third segment to a bent wire with no constraint on its orientation yields about the same extremes of  $\beta_{xxx}$  and  $\gamma_{xxx}$  as the two-wire graph. Imposing geometrical constraints on the third edge causes minor quantitative change, as can be seen in the line triangles with open vertices in Table I. The addition of even more degrees of freedom enables wire configurations of optimum shape to be marginally improved and provides limited enhancement of nonlinearities. For bent wires,  $\gamma_{xxx}$  can be positive or negative. The eigenstates of bent wires are non-degenerate, a consequence of the open topology for the graph.

The separation of geometrical and topological factors displayed in Eq.(3) practically begs for an expansion of the hyperpolarizabilities into irreducible, spherical

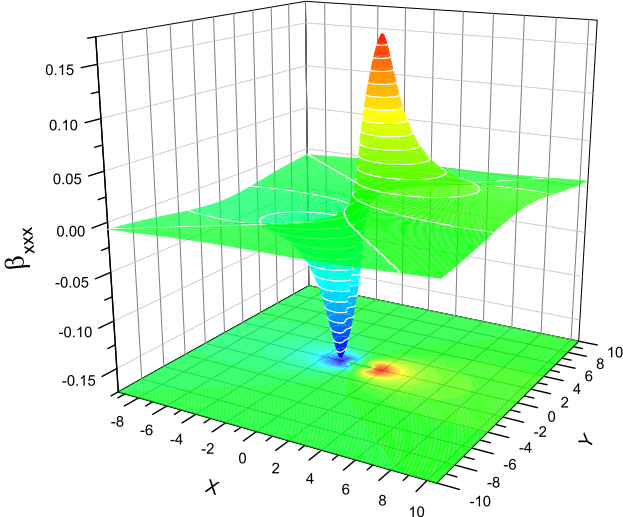


FIG. 1. Hyperpolarizability of a bent wire that is defined by the coordinates  $(0,0)$ ,  $(x,y)$  and  $(1,0)$ .

tensors[14, 15] in order to visualize the geometrical and topological effects across structures. For fully symmetric tensors,  $\beta_{ijk}$  is represented by the spherical tensors  $\beta_1$  and  $\beta_3$  – corresponding to  $J = 1$  and  $J = 3$  irreducible representations, while  $\gamma_{ijkl}$  has nonzero  $\gamma_0$ ,  $\gamma_2$ , and  $\gamma_4$  – corresponding to  $J = 0$ ,  $J = 2$ , and  $J = 4$  irreducible representations. Detailed expansions are available in the literature [16]. The tensor norms are given by  $|\beta|^2 = |\beta_1|^2 + |\beta_3|^2$ , and  $|\gamma|^2 = |\gamma_0|^2 + |\gamma_2|^2 + |\gamma_4|^2$ ; and, are identical to those computed in Eq.(1).

Consider first the closed-loop topologies from Table I. The solutions are a doubly-degenerate set of modes with a singlet ground state at zero energy and a periodic boundary condition on the eigenstates. (Note that a complex quadrilateral has the same topology as a simple quadrilateral when the crossing edges do not transfer probability flux, as we assume here).

The closed-loop topology severely limits the magnitudes of the first hyperpolarizability across the set of geometries. Compared to a simple bent wire, a triangle loop is a poorer nonlinear optical structure with a maximum  $\beta_{xxx} \sim 0.049$ . More significant, the second hyperpolarizability  $\gamma_{xxxx}$  is always less than or equal to zero in closed-loop graphs. Finally, rapid saturation of the nonlinearity with the number of edges occurs, as it did for bent wires. Large  $\beta_{xxx}$  is associated with open, isosceles-like shapes, while low-aspect ratio (flat) triangles yield zero  $\beta_{xxx}$ . But  $\gamma_{xxxx}$  is the most negative for flat triangles. Quadrangles and above may be geometrically squeezed into these shapes, thus explaining how the topological features of the loops drive most of the physics, while the geometric shapes have only a modest effect.

Figure 2 compares the tensor properties of the distribution of 10,000 random samples of configurations of the closed-loop triangle and quadrangle graphs shown in Ta-

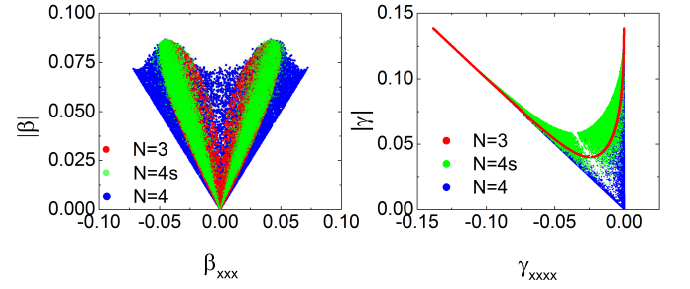


FIG. 2.  $|\beta|$  vs  $\beta_{xxx}$  and  $|\gamma|$  vs  $\gamma_{xxxx}$  for 10,000 randomly-sampled graph configurations of fixed topology. Quintangle results are not shown, as their tensors look almost identical to the quadrangles.

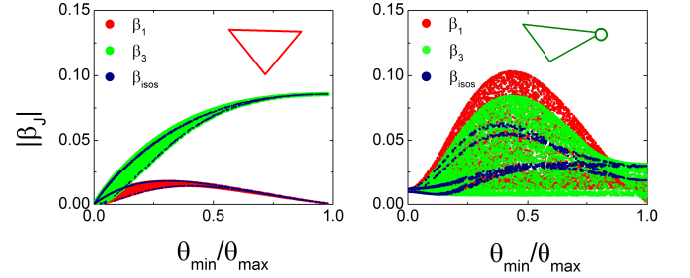


FIG. 3. Spherical tensors for  $|\beta|$  as a function of the ratio of the smallest angle  $\theta_{min}$  to the largest angle  $\theta_{max}$  in a closed loop (left) and open (right) triangle graph.

ble I. (Note that all plots that follow use 10,000 random samples.) The plot on the left shows  $|\beta|$  vs  $\beta_{xxx}$ , while the plot on the right shows  $|\gamma|$  vs  $\gamma_{xxxx}$  for the three (fixed topology) geometrically-different closed loops. Triangle graphs, which have only two angular degrees of freedom, have large (absolute) projections onto the x-axis only when  $|\beta|$  is large as well. The quadrilateral, having 3 degrees of freedom, has the largest value of  $\beta_{xxx}$ , but marginally so. When  $|\beta|$  has its largest value,  $\beta_{xxx}$  is not optimal. However,  $|\beta|$  is maximum for the same values of  $\beta_{xxx}$  in all geometries.

The constraint imposed by the closed triangular loop on the second hyperpolarizability yields a tight grouping of all configurations, as shown by what appears to be a smooth red curve. Adding extra degrees of freedom yields a greater spread in  $|\gamma|$  for a given value of  $\gamma_{xxxx}$ , as is also found for the first hyperpolarizability. However,  $\gamma_{xxxx}$  is at its minimum and maximum when  $|\gamma|$  is at its maximum. When  $|\gamma|$  is minimum,  $\gamma_{xxxx}$  appears to be minimum only in the limit of an infinite number of degrees of freedom.

In summary, the range of  $\beta$  and  $\gamma$  over all configurations is limited by the loop topology, not the geometry.

Figure 3 shows a plot of the contributions to  $|\beta|$  from the two spherical tensors for a closed triangle and an open vertex triangle. For closed loops, large  $|\beta|$  graphs are dominated by the  $\beta_3$  tensor when  $\theta_{min} = \theta_{max}$  implying that  $\beta$  is maximal for an equilateral triangle. The black

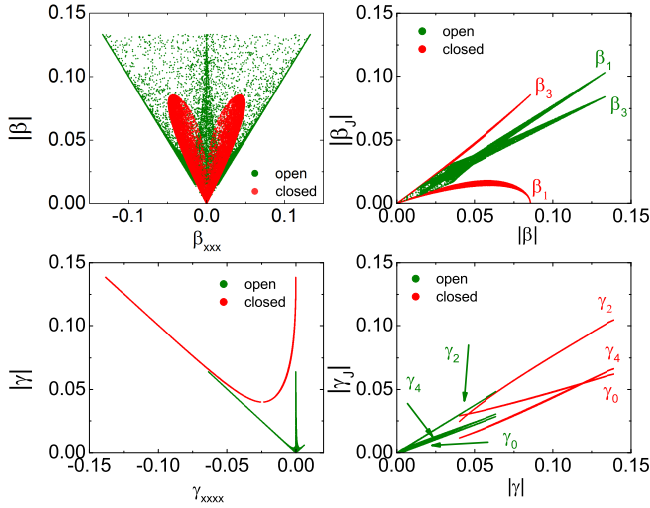


FIG. 4. Topological dependence for fixed geometry. The figures show the variation in the hyperpolarizability tensor components and their norms for open and closed triangle graphs.

points are for isosceles triangles. The conclusion is that high aspect ratio triangles have near-zero  $\beta_{xxx}$  regardless of their orientation.

For triangles with an open vertex, corresponding to a change in topology from the closed triangle, the relationship between the spherical tensor components and the angle ratio are profoundly different.  $\beta_1$  exceeds  $\beta_3$  and  $|\beta|$  is substantially larger for the open vertex triangles. Furthermore, isosceles triangles no longer give the largest  $\beta$  and the equilateral triangle has smallest  $|\beta|$ , compared with largest  $|\beta|$  in the case of the closed triangle. Topology therefore has a profound effect on both the magnitude and character of the first hyperpolarizability.

The profound effect of topology on the first and second hyperpolarizability is emphasized in Figure 4. For the closed loop, both  $\beta_{xxx}$  and  $|\beta|$  are smaller; and, the range of  $\beta_{xxx}$  is substantially less than for  $|\beta|$ . When a vertex is opened,  $\beta_{xxx}$  and  $|\beta|$  are both larger, and there exists a configuration for which  $\beta_{xxx} = |\beta|$  for all  $|\beta|$ . The opposite is true for  $\gamma$ . The closed configuration yields the largest value of  $|\gamma|$  and  $\gamma_{xxxx}$ . Additionally, the same span of geometrical configurations for each leads to divergent behavior as shown in the figures.

$\beta_1$  is always smaller than  $\beta_3$  in the closed triangle but are both comparable in the open one. The second hyperpolarizability  $\gamma$  is dominated by  $\gamma_2$  in all cases, and each  $\gamma_i$  in the loop topology approximately parallels  $\gamma_i$  in the open vertex case; but, the values of  $\gamma_i$  are larger for the loops.

These observations can be understood as follows. Opening a single vertex in a closed triangle removes half the eigenstates and shifts the ground state to nonzero energy. The result is a shift in the vector component of  $|\beta|$  from an insignificant contributor in closed triangles to a substantial contributor for the open triangles. The topological change causes two significant changes in

$\gamma_{xxxx}$ , as it allows for configurations with exactly zero norm as well as shapes with positive  $\gamma_{xxxx}$  for open triangles. Though geometrically identical, the closed and open topologies differ by over a factor of three in  $\beta_{xxx}$ , and the open triangles have configurations with positive  $\gamma_{xxxx}$ .

For simple quadrangles, the distribution of  $\gamma$  fills a greater area in the  $|\beta_J| - |\beta|$  plane than for triangles, reflecting the additional degree of freedom in its configuration space. In a triangle, two angles define a set of similar triangles – all having the same geometry and same intrinsic nonlinearities. In a quadrangle, three angles do not form a unique similarity class, leading to a greater spread of intrinsic nonlinearity. The additional degrees of freedom afforded to a general quadrangle fills even a greater part of the plane, yet  $\beta_{xxx}$  increases only modestly with increasing degrees of freedom. The loop topology constrains  $\beta_{xxx}$  to values well under that of the simple bent wires and keeps  $\gamma_{xxxx}$  negative for any shape.

Table I summarizes these results and compares the closed-loop topology with three line configurations, each of which is a bent wire or a composite of bent wires discussed previously. Opening a single vertex in a closed-loop triangle eliminates the eigenstate degeneracies and produces a ground-state with nonzero energy. The bent wire triangle with one open vertex and no flux circulation has a much larger  $\beta_{xxx} \sim 0.133$ , and a positive, maximum  $\gamma_{xxxx}$ . In these triangle graphs, the extremes of  $\beta_{xxx}$  and  $\gamma_{xxxx}$  occur for the opposite geometries of those in the closed-loop triangle.

To quantify the geometrical effect of the ‘openness’ of a loop, we define the dimensionless geometrical parameter  $\xi$  as the ratio of the area of a loop to the square of its perimeter. Since a polygon with all edge lengths equal to each other and all angles equal to each other has maximum  $\xi$ , we normalize all  $\xi$  to this value to get the intrinsic geometric parameter. Fig. 5 shows  $|\beta|$  and  $|\gamma|$  (normalized to unity) as a function of  $\xi$  for both closed (loop) and open (bent wire, one vertex open) triangles. The black points in the Figure are isosceles-like triangles and  $\xi = 1$  is an equilateral triangle. Opening a second vertex in the bent-wire triangle increases the  $\beta_{xxx}$  toward that of a bent wire while still yielding positive  $\gamma_{xxxx}$  configurations. Opening all vertices produces three single wires, for which  $\beta_{xxx}$  is exactly zero and  $\gamma_{xxxx}$  approaches the value it has for a single bent wire. In such systems, the eigenstates are constructed from three 1-wire graphs by ordering the individual energies of each wire to form the composite and demanding that superpositions maintain unitarity.

The final set of graphs in Table I, the so-called star graphs, are fundamentally different than any discussed so far. The 3-prong star graph is an irregular graph with four degrees of freedom (two angles and the lengths of two edges), providing much larger nonlinearities than any of the regular graphs. The spectra of the 3-prong topology has been solved in closed form using a periodic orbit expansion [17], and properties of the eigenfunctions have



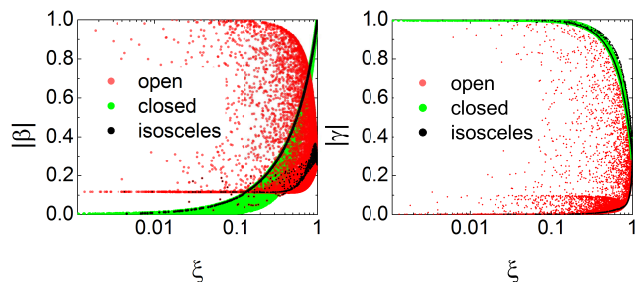


FIG. 5. Scaling of  $|\beta|$  (left) and  $|\gamma|$  (right), both normalized to unity, as a function of geometric parameter  $\xi$ , for closed- and open-loop topologies. The black points represent isosceles-like geometries.

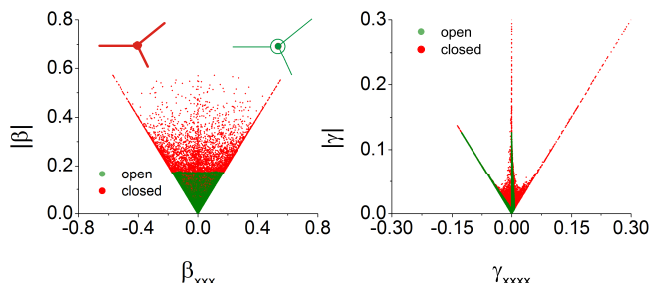


FIG. 6. Topological dependence for fixed geometry of star graphs, showing on the left (right) a very large enhancement in  $\beta_{xxx}$  ( $\gamma_{xxxx}$ ) for the closed star with three attached prongs (red) compared to the same graph with one prong detached (green).

been studied [18]. For nonlinear optics, a numerical solution of the secular equation for the star graph wave equation provides the simplest way to get the energies and eigenfunctions required to compute the dipole moment matrix for use in the sum-over-states construction of  $\beta_{xxx}$

and  $\gamma_{xxxx}$ . The result is a maximum  $\beta_{xxx}$  of order 0.55, over half of the fundamental limit and the largest calculated to date for any simple structure. Fig 6 illustrates the dramatic change caused by a simple topological shift in a graph from three connected prongs to two. To the extent that stars are effective nano-wire[19] and molecular models, they could provide the molecular designer and nano-technologist[20] with guidelines for achieving breakthroughs in nonlinear optics. As expected, a major change in the topology of the star graph by opening a prong at the central vertex changes the highly-active 3-fork into a graph resembling a bent wire system. An obvious conclusion of this analysis is that combinations of simple structures such as bent wires and stars may lead to structures with even larger nonlinear optical response. More complex structures are under study.

In summary, we have presented for the first time an exact, quantitative dependence of the nonlinear optics of quantum graphs on their geometry and topology. We have shown that the effects of the topology of geometrically similar graphs dominate those of the geometry of topologically similar graphs. Topology largely determines the eigenstates and spectra, whereas the geometry mainly affects the projections of the graph edges in the  $x-y$  plane. Closed loop graphs always have non-optimum  $\beta_{xxx}$  and negative  $\gamma_{xxxx}$ , but opening a vertex immediately raises  $\beta_{xxx}$  by over a factor of three and enables graphs with positive  $\gamma_{xxxx}$ . We have also verified that additional degrees of freedom enhance the nonlinearity of the graph, unless a fundamental topological constraint is in place, such as a closed loop boundary condition on the eigenstates. Finally, we have shown that the star graph has the largest intrinsic hyperpolarizability calculated to date in a simple quantum system.

SS, JS and MGK thank the National Science Foundation (ECCS-1128076) for generously supporting this work.

- 
- [1] T. Kottos and U. Smilansky, Phys. Rev. Lett. **79**, 4794 (1997).
  - [2] T. Kottos and U. Smilansky, Ann. Phys. **274**, 76 (1999).
  - [3] R. Blümel, Y. Dabaghian, and R. V. Jensen, Phys. Rev. Lett. **88**, 044101 (2002).
  - [4] R. Blümel, Y. Dabaghian, and R. V. Jensen, Phys. Rev. E **65**, 046222 (2002).
  - [5] Y. Dabaghian and R. Blümel, Phys. Rev. E **70**, 046206 (2004).
  - [6] Y. Dabaghian, R. Jensen, and R. Blümel, J. Exp. Theo. Phys. **94**, 1201 (2002), 10.1134/1.1493174.
  - [7] Y. Dabaghian and R. Blümel, Phys. Rev. E **68**, 055201 (2003).
  - [8] M. G. Kuzyk, Phys. Rev. Lett. **85**, 1218 (2000).
  - [9] B. J. Orr and J. F. Ward, Molec. Phys. **20**, 513 (1971).
  - [10] S. Shafei and M. G. Kuzyk, J. Opt. Soc. Am. B **28**, 882 (2011).
  - [11] S. Shafei and M. G. Kuzyk, J. Nonl. Opt. Phys. Mat. **20**, 427 (2011).
  - [12] M. G. Kuzyk, Phys. Rev. A **72**, 053819 (2005).
  - [13] M. G. Kuzyk, Phys. Rev. Lett. **90**, 039902 (2003).
  - [14] J. Zyss and I. Ledoux, Chem. Rev. **94**, 77 (1994).
  - [15] M. Joffe, D. Yaron, J. Silbey, and J. Zyss, J. Chem. Phys. **97**, 5607 (1992).
  - [16] J. Jerphagnon, D. Chemla, and R. Bonneville, Adv. Phys. **27**, 609 (1978).
  - [17] Z. Pastore and R. Blümel, J. Phys. A **42**, 135102 (2009).
  - [18] J. Keating, J. Marklof, and B. Winn, Comm. Math. Phys. **241**, 421 (2003), 10.1007/s00220-003-0941-2.
  - [19] R. Yan, D. Gargas, and P. Yang, Nature Photonics **3**, 569 (2009).
  - [20] H. Yan, H. Choe, S. Nam, Y. Hu, S. Das, J. Klemic, J. Ellenbogen, and C. Lieber, Nature **470**, 240 (2011).